

# A dynamic test methodology for determining the longitudinal compressive response of carbon fiber composite tows

Jiahui Gu<sup>1,3</sup>, Yang Bai<sup>1,3</sup>, Zhenqiang Zhao<sup>1,3\*</sup>, Chao Zhang<sup>1,2,3\*</sup>

<sup>1</sup>School of Aeronautics, Northwestern Polytechnical University, Xi'an, Shaanxi 710072, China <sup>2</sup>School of Civil Aviation, Northwestern Polytechnical University, Xi'an, Shaanxi 710072, China <sup>3</sup>Joint International Research Laboratory of Impact Dynamics and Its Engineering Application, Xi'an, Shaanxi 710072, China

#### **Abstract**

Textile composites have been applied widely in aircraft structures, such as fan blades and cases of aero-engine, because of their excellent impact resistance, great delamination resistance and high damage tolerance. Composite fiber tows, as the main load-bearing component, have a critical influence on the dynamic performance of textile composites and even the whole composite structures. However, the determination of the intrinsic properties of individual composite tow mainly relies on theoretical and numerical predictions. In this study, a dynamic compression test method for composite fiber tows is proposed based on the Split Hopkinson pressure bar system combined with an ultra-high-speed camera. Firstly, the porosity contents of composite tows are evaluated and characterized to compare the influence of different preparation methods. A reasonable dumbbell-shaped configuration for the compressive specimen is then proposed, based on the results of both simulated and experimental validation on the stress distribution, the data reduction method, dynamic stress balance, and failure morphology. The preliminary test results show that the compressive properties of composite tows are significantly dependent on the strain rates, and the compressive strength increases by nearly 90% when the strain rate ranges from 0.01 s<sup>-1</sup> to 400 s<sup>-1</sup>. This work will realize the direct and efficient test methodology for determining the dynamic longitudinal compressive performance of composite tows and provide insightful inputs for multiscale analysis of textile composite.

Keywords: Composite tows; testing methodology; dynamic compression; strain-rate effect

#### 1. Introduction

Textile composites, prized for their impact resistance and out-of-plane performance, are well-suited for aerospace and industrial structures. Given their exposure to potential impact loads, understanding strain-rate dependence on mechanical behaviors of textile composite is crucial during structural design. The primary component of the textile composite meso-structure is the composite tows, which are micro unidirectional (UD) composites formed after the dry fiber tows (bundles) are resin-impregnated and cured. The axial mechanical properties of these composite tows significantly influence the overall mechanical response of textile composites. Thus evaluating the strain-rate sensitivity of composite tows is essential for accurately describing the dynamic mechanical behavior of textile composites [1]. Currently, assessing strain-rate sensitivity of composite tows relies mainly on the inversion of macroscopic experiments, with limited direct research on the dynamic compression of composite tows. The longitudinal compressive behavior of UD composites is influenced by factors like load application, boundary conditions, and internal defects, leading to lower mechanical properties compared to longitudinal tensile behavior. Standardized quasi-static compression tests sometimes inadequately represent true compression strength due to premature failure. Dynamic compression results are further affected by factors such as stress concentration and inertial effects. Consequently, evaluating compression properties and strain rate effects in unidirectional composites heavily depends on the

test method, with varying reported results from different authors. Hsiao and Daniel [2] used a drop tower to study 0° composites, showing the increased strength and elastic modulus at high strain rates. Ploeckl et al. [3] reported an almost rate-independent elastic modulus and up to a 40% strength increase at 119 s-1. Rouf et al. [4] achieved consistent results. However, differences and controversies in these studies highlight the ongoing challenges in establishing a reliable dynamic longitudinal compressive test for UD laminates. Given that composite tows are mesoscale specimens, complicating buckling resistance, strain measurement, and load application, the methods based on laminate specimens are not directly applicable for composite tows, but few experimental studies have been conducted on the dynamic compressive performance of composite tows.

This study aims to develop a test method for evaluating the compressive response of composite tows, offering an effective and reliable approach to analyze their strain rate dependence. Experimental characterization was used to evaluate the quality of the composite tows made from different manufacturing methods. An effective dumbbell-shaped specimen configuration was proposed after finite element (FE) analysis. The applicability of the specimen configuration and the data processing method was meticulously verified through a combination of tests and finite element simulations. Lastly, the compressive response and failure characterization of the composite tows at different strain rates were analyzed and discussed.

## 2. Specimens manufacture and designs

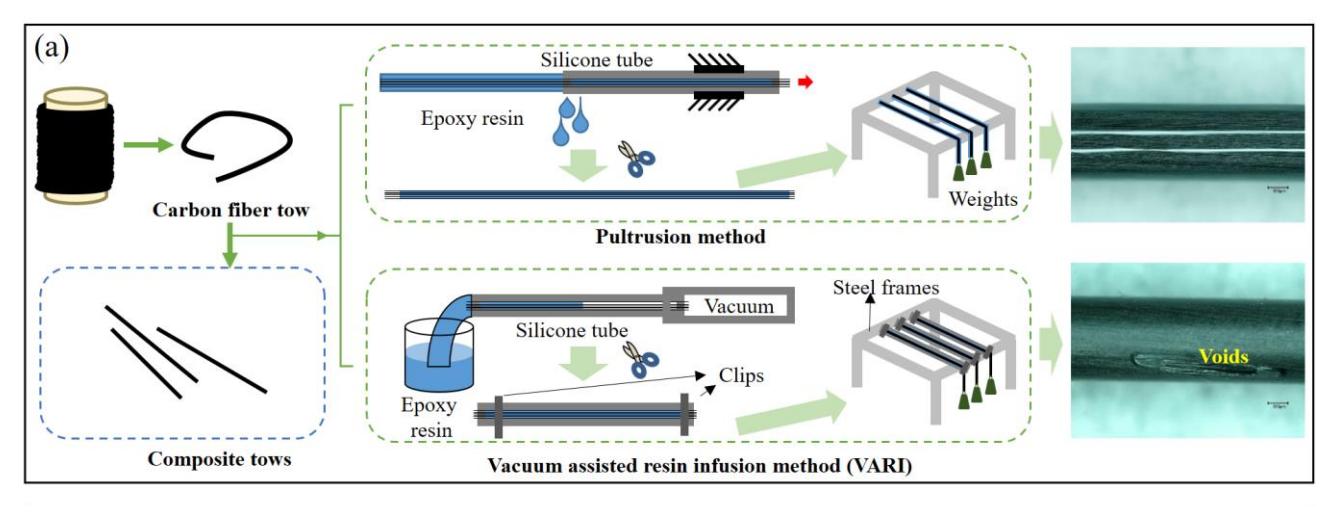
## 2.1 The manufacturing method for Composite tows

This study compares two manufacturing methods for composite tow, illustrated in Figure 1(a), known as pultrusion and vacuum assisted resin infusion method (VARI). The raw materials are carbon fiber multifilament HTS40-12K and epoxy resin MIMR036. In the pultrusion method, a length of dry fiber tows is initially impregnated in a container full of liquid epoxy. The impregnated tow is then passed through a silicone tube to extricate excess epoxy and shape the cross-section. Subsequently, the impregnated tow is hung on a steel frame, straightened with a weight, and cured at 70°C for 10 hours. In the VARI method, dry carbon fiber tow is pre-inserted into a silicone tube, and heated with a heat gun to shrink to an inner diameter of 1.2 mm. Then, one end of the silicone tube is immersed in the resin pot, and the other end is connected with a vacuum degassing pot to inject the resin into the silicone tube. The end of the fiber tow in the resin pot is fixed to the bottom of the resin pot with sealant tape to reduce movement during the injection process. Once resin infusion is completed, both ends of the silicone tube are tightened to avoid resin leakage and air intake. The subsequent straightening and curing process is identical to that employed in the pultrusion method.

The quality of the composite tows from these two methods was characterized. The prepared composite tows were embedded in epoxy resin and then sectioned into at least 15 segments along the fiber direction. These segments were meticulously polished using SiC sandpaper and  $Al_2O_3$  powder suspension in a rotary polishing machine. The void volume fraction and its distribution in each sample were statistically measured by the image recognition process. It was observed that the VARI method produced more surfacial voids compared to the pultrusion method, as depicted in Figure 1(a). This difference may be attributed to the residual air inside the fiber tow being confined around internel surface of the tube during the curing process in the VARI method. The average void content for the pultrusion method and VARI method was found to be 1.26% and 1.51%, respectively. Statistical results indicated that the majority of voids obtained by both methods were less than 2  $\mu$ m. However, the pultrusion method resulted in lower porosity and a lower frequency of large pores, resembling common UD composite products. Consequently, the pultrusion method is recommended as a feasible process for the preparation of composite filaments.

The specimen configuration was designed with an emphasis on manufacturing efficiency and accuracy. Considering the small diameter of the composite tow (1.2mm), common end tabs and bonding processes, which are difficult to keep stable, were abandoned. The preparation of the specimen is shown in Figure 1(b). First, a composite tow was vertically inserted into a tube mold, with the upper and lower ends constrained by the bottom and top caps to ensure coaxial alignment with the tube. Subsequently, epoxy resin was poured into the tube mold and cured, resulting in an epoxy cylinder with the composite tow embedded in the center. This epoxy cylinder was then machined into a dumbbell shape through a turning process. It is important to note that the gauge section of the

composite tow was still left with a thin resin layer to prevent processing damage. The detailed geometric dimensions of the specimen design are indicated in Figure 1(b), and the specific dimensional determination will be discussed in Section 2.2.



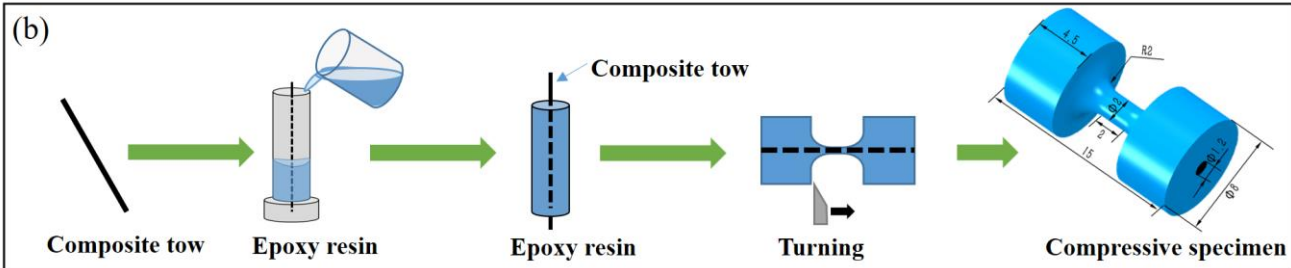


Figure 1 – (a) Comparison of two manufacturing methods of composite tows; (b) schematic diagram of specimen configuration preparation and its dimensions.

#### 2.2 Specimen configuration design

To further evaluate and analyze the stress distribution in the gauge section, which is sensitive to compression performance, FE models for different specimen configurations were built and solved in Abaqus/Standard and their specific geometric dimensions are shown in Figure 2(a). The models were assembled in two rigid plates as the top rigid plate was applied with a concentrated compression force of 1500 N, and the bottom rigid plate was fixed. Eight-node brick element with reduced integration (C3D8R) was adopted in all models. In addition, the composite tow was considered as transversely isotropic elastic material, and its engineering constants of  $E_1 = 99.8$  GPa,  $E_2 = E_3 = 6.2$  GPa,  $E_3 = 2.3$  GPa,  $E_3 = 1.8$  GPa,  $E_4 = 1.8$  GPa,  $E_5 = 1.8$  GPa,  $E_7 = 1.8$  GPa,  $E_7$ 

For the dumbbell-shaped specimen configuration, in addition to the length of the gauge section, which has been determined to be 2 mm, Figure 2(a) depicts the remaining key geometrical parameters affecting the testing of its mechanical properties. These include the radius (R) of the transition chamfer, the outer diameter (d) of the gauge section and the bottom outer diameter (D). To compare the effect of these parameters on the stress distribution of specimens subjected to compression, especially  $S_{11}$  and  $S_{12}$ , each parameter is divided into three levels for simulation and comparison.

The variations in stress distribution concerning R, d, and D are illustrated in Figure 4(b) to (d), respectively. From Figure 4(b), it is evident that as the R increases from 0 to 2 mm, the maximum shear stress on the central axis of the gauge section (indicated by the red dashed path) decreases significantly, dropping from approximately 35 MPa to 2 MPa. This substantial decrease mitigates the concentration of shear stress in the resin layer and the gauge section of the composite tow. In Figure 4(c), the change in the distribution of longitudinal compressive stress S<sub>11</sub> is depicted as the outer diameter of the pitch section d increases from 1.2 mm to 4 mm. This increase results in a significant

reduction in the compressive stress level of the gauge section. However, it also leads to more uniform compressive stress in the gauge section at the medial axis. Nonetheless, excessively thick resin layers increase the risk of premature end failure. The outer diameter D of the end, shown in Figure 4(d), directly affects the stress level of the end. When D is 4 mm, the local compressive stress at the bottom of the end reaches a magnitude comparable to that of the gauge section. This is likely to lead to compression failure at the non-gauge section. The results of the FE analysis preliminarily indicate that the geometrical parameters of the specimen configuration are interdependent and should be carefully verified. After these analyses, the acceptable geometric configuration of the composite tow in this study is the chamfer radius R of 2 mm, the outer diameter d of 2 mm in the gauge section, and the end diameter D of 8 mm, which need further validation by experiments.

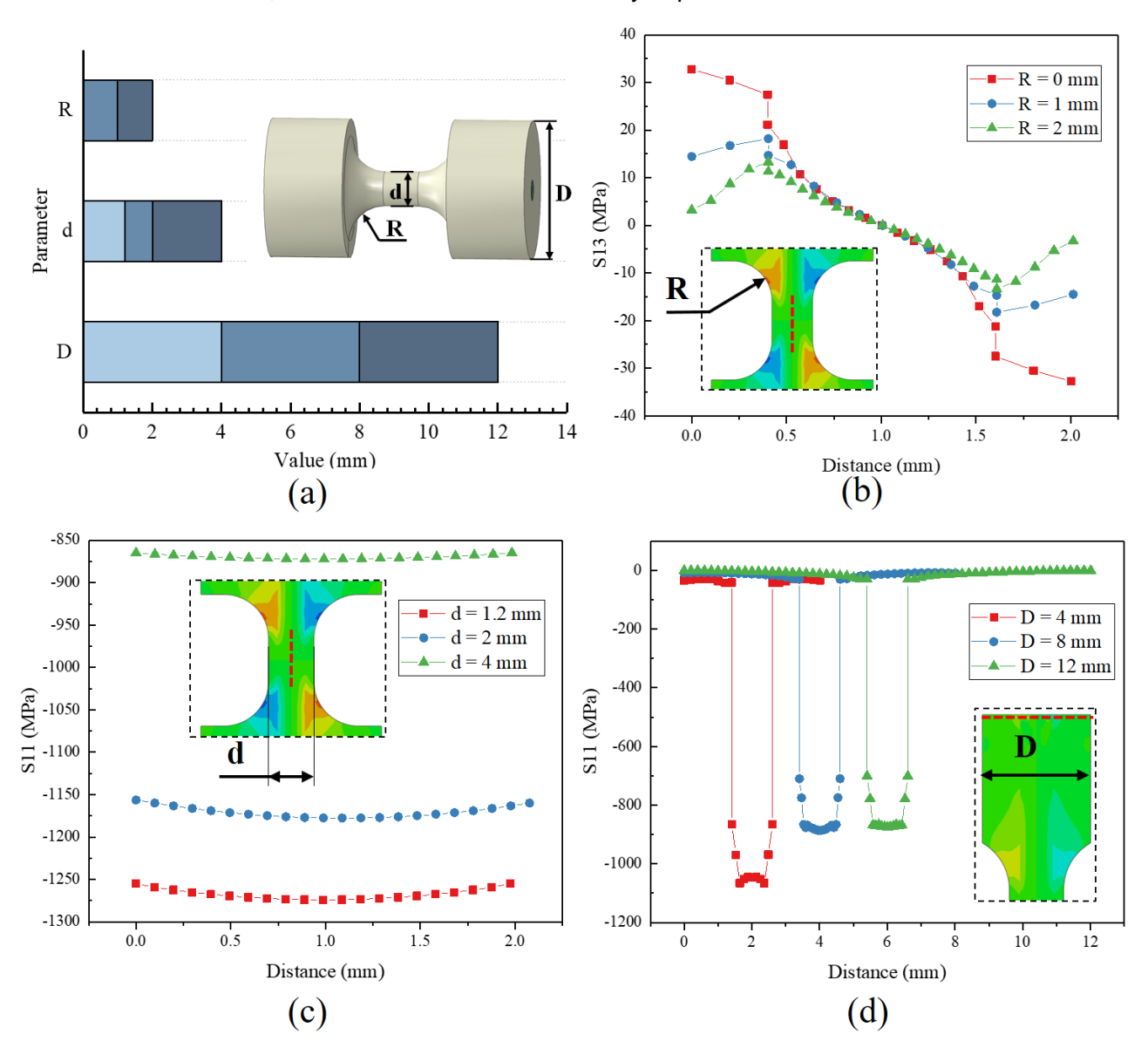


Figure 2 – The effect of specimen geometrical parameters in simulation: (a) parameter adjustment scheme; (b) the transition chamfer R; (c) the outer diameter d of the gauge section; (a) the bottom outer diameter D.

## 3. Compressive equipment and method validation

## 3.1 Quasi-static and dynamic compressive setup

Quasi-static compression tests were performed using an Instron 5848 mechanical testing machine, operating at a loading speed of 0.02 mm/s in Figure 3(a). Force-displacement data were acquired at a frequency of 10 Hz. To minimize potential load imperfection, custom-designed fixtures were

employed, comprising a rigid steel frame, two linear bearings, and compression heads, as depicted in Figure 3(a). Subsequently, black and white spots were sprayed onto the specimens, and a digital camera with  $500 \times 800$  pixels was utilized to record the surface deformation process of the specimen during the test at a rate of 5 frames per second. The axial strain was then post-processed using the DIC analysis software.

The Hopkinson pressure bar system comprises several key components: the gas chamber, striker bar, incidence bar, transmission bar, strain acquirement system, dynamic digital oscilloscope (GEN3i, HBM Ltd.), high-speed camera system (Kirana 05M, Specialized Imaging Ltd.), and personal computers, as illustrated in Figure 3(b). Both the incident and transmitted bars are made of titanium alloys with a diameter of 13 mm and corresponding lengths of 1500 mm and 1200 mm, respectively. During the experiment, the composite tows specimen was positioned between the incident bar and the transmitted bar. A spot of petroleum jelly was applied to the front and rear surfaces of the specimen before assembly. A pulse shaper, consisting of a plasticine ball with a 2-mm diameter, was utilized to achieve a smoother rising edge of the incident wave and to reduce pulse oscillations. The deformation and failure process of the specimen was captured using a high-speed camera, which is capable of capturing 180 pictures at a frame rate of one million frames per second. Following the initial impact, the incident stress waves generated on the front of the incident bar and propagated back to the transmission bar were transformed into reflected and transmitted waves. The electrical signals from the strain gauges were recorded by an oscilloscope at a frequency of 10 MHz.

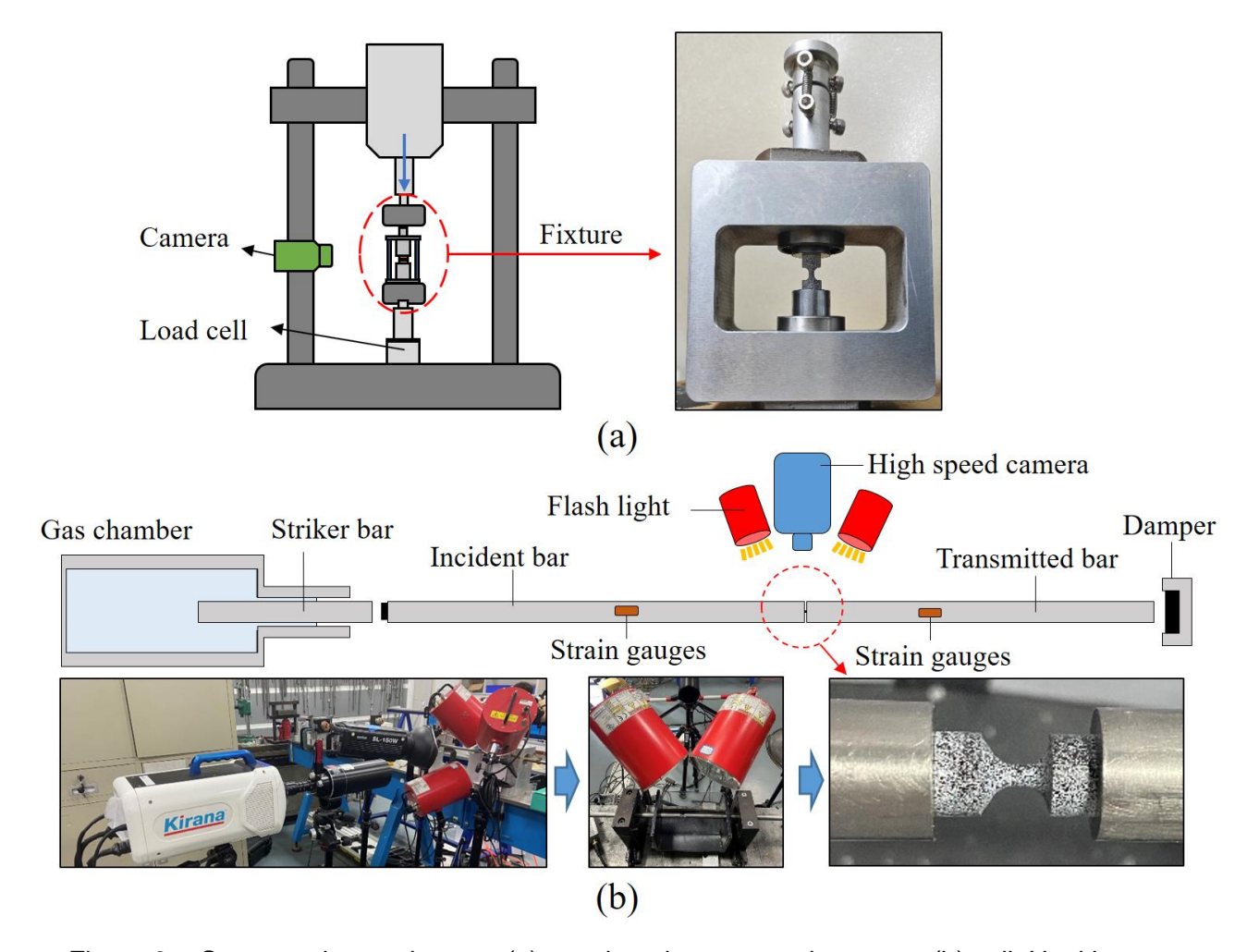


Figure 3 – Compressive equipment: (a) quasi-static compressive setup; (b) split Hopkinson pressure bar system.

Once the incident, reflected, and transmitted signals of the Hopkinson bar are analyzed using classical one-dimensional stress wave analysis, we can derive the engineering stress  $\sigma(t)$ , engineering strain

 $\varepsilon(t)$ , and engineering strain rate  $\dot{\varepsilon}(t)$  of the specimen.

$$\sigma(t) = \frac{AE}{A_{\rm s}} \varepsilon_{\rm T}(t) \tag{1}$$

$$\varepsilon(t) = \frac{-2C}{L_s} \int_0^t \varepsilon_R(t)$$

$$\dot{\varepsilon}(t) = \frac{-2C}{L_s} \varepsilon_R(t)$$
(2)

$$\dot{\varepsilon}(t) = \frac{-2C}{L_{\rm s}} \varepsilon_{\rm R}(t) \tag{3}$$

where  $\varepsilon_R(t)$  and  $\varepsilon_T(t)$  are reflected, and transmitted strain pulses, respectively. A, E, and C respectively present the sectional area, elastic modulus, and wave velocity of bars. Ls and As present the gauge length and sectional area of the composite tow respectively.

#### 3.2 Method validation and data reduction

During dynamic testing, the non-gauge section of the dumbbell specimen also contributes to the whole deformation and the resin layer in the gauge section also shares the whole compressive loads somehow. Therefore, the strain and stress calculated by Equation (1) - (3) should be corrected. it is essential to establish a precise finite element model that reflects the specimen response during dynamic loading and to validate strain and stress correction methods. Thus the incident bar, specimen, and transmission bar were modeled with 1/4 symmetry in ABAQUS/Explicit, matching the experimental dimensions. Asymmetric displacement boundary condition was applied on symmetric surfaces, and a contact penalty friction coefficient of zero was set between the specimen and bars. The same stress wave pulse used in the experiment was applied at the front end of the incident bar. The mechanical properties of resin matrix maintain the same outlined in Section 2.2 and takes ductile damage into account furthermore. The engineering constant of the composite tow remained consistent with Section 2.2. Longitudinal compressive strength of the composite tow was set to 1400 MPa, the similar strength in dynamic tests, and the remaining strengths were also determined using Huang's bridging model. Damage initiation and evolution of the composite tows were described by the Hashin-Hou failure criterion [7], [8] and the Murakami-Ohno damage theory [9], implemented in ABAQUS through a userdefined subroutine VUMAT. For more comprehensive details on the progressive damage model of the composite tow, please refer to our previous work [10].

Figure 4(a) compares the typical strain wave pulses in both the experiment and the FE model. The model accurately replicates the actual stress wave reflection and transmission process. Slight differences in the transmitted signal arise from variations between the assumed strength in the model and the actual compression strength of the composite tow. The transient platform on the reflected wave suggests that the specimen reach a constant strain rate during loading. The assumption in Equations (1) - (3) in the SHPB test, that the specimen achieves stress equilibrium at both ends, generally poses challenges for brittle composites. To check this, the averaged stresses of the incident and transmission bar end in the simulation are extracted, and the stress equilibrium coefficient  $\alpha(t)$  is calculated using:  $\alpha(t) = |2[\sigma_1(t) - \sigma_2(t)]/[\sigma_1(t) + \sigma_2(t)]|$ . The results are presented in Figure 4(b). As the stress wave reflects back and forth in the specimen, the stress equilibrium coefficient  $\alpha(t)$  rapidly oscillates from an initial value of nearly 200% to less than 5%, with this critical value considered to signify stress equilibrium [11]. At this point, the average engineering stress of all composite tow element in the gauge section remains below 600 MPa, indicating that the composite tow can early achieve stress equilibrium during dynamic loadings, fulfilling a fundamental assumption of SHPB.

When computing stress, strain, and strain rate in SHPB tests, it is crucial to modify Equations (1) - (3) to precisely capture the response of the composite tow. In terms of strain correction, some slight deformation occurs in the non-gauge section of the specimen should be eliminated. Consequently,  $L_{\rm s}$ in Equation (2) cannot be assigned to the actual length of the gauge section but an equivalent length. The simulation results from the FE model show  $L_s$  of 12.5 mm will be suitable since the average straintime curve of all elements in the gauge section corresponds with the calculated results from Equation (2) with the  $L_{\rm s}$ .

The resin layer of the gauge section also contributes to the global compressive load, thus necessitating the modification of the stress  $\sigma_f$  of the composite tow by the simple rule of mixture in Equation (4):

$$\sigma_{\rm f}(t) = \frac{AE}{A_{\rm s}} \varepsilon_{\rm T}(t) - \frac{A_{\rm m} E_{\rm m} \varepsilon_{\rm m}}{A_{\rm s}} \tag{4}$$

where  $A_{\rm m}$ ,  $E_{\rm m}$ , and  $\varepsilon_{\rm m}$  are sectional area, elastic modulus and compressive strain of resin matrix layer,

### respectively.

We have corrected the strain and stress in the SHPB analysis depicted in Figure 4(a), and the results presented in Figure 4(c) indicate that the response of the composite tow obtained after SHPB calculation closely mirrors the average response of all elements in the gauge section of the composite tow, effectively eliminating the influence of the resin layer. As a result, the proposed correction method for dumbbell-shaped specimens has been validated.

After comparing the deformation failure process of the composite tow in the simulation and the experiment, it was observed that as the composite tow gradually reached peak stress, the specimen experienced compression failure first in the gauge section, accompanied by plastic deformation and cracking of the local resin layer. Hence, the FE model effectively replicated the deformation and failure process captured by the high-speed camera during the test, thus fully verifying the accuracy of the simulation model, in addition to accurately predicting the mechanical response of the specimen.

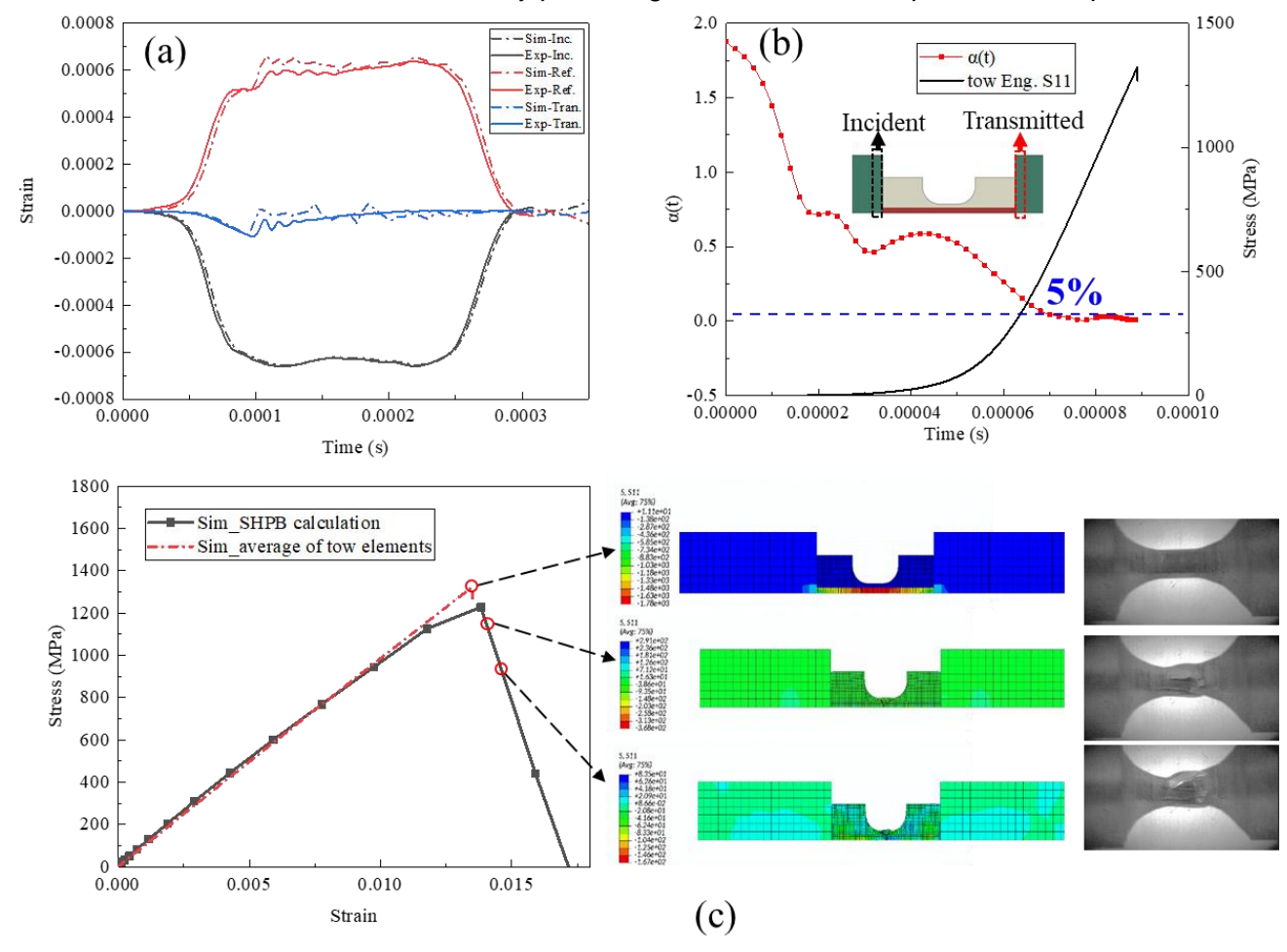


Figure 4 – (a) typical incident-, reflected- and transmitted strain pulse of SHPB in the test and simulation; (b) the stress equilibrium check of SHPB results; (c) comparison between the corrected and averaged response of the simulation and test.

## 4. Experimental results and discussion

Figure 5(a) depicts the stress-strain response curves of three composite tow specimens under quasistatic loading (strain rate of  $0.01~\text{s}^{-1}$ ). As the strain increases, the longitudinal stress of the specimen exhibits a clear linear increase until catastrophic sudden failure. The peak stress and corresponding strain are considered as the compressive strength and failure strain of the composite tow, respectively, and the compressive modulus are obtained by linear fitting of the initial segment within a strain range of less than 0.6%. Upon data reduction, the average longitudinal compressive strength of the quasistatic composite tow is  $975.88 \pm 51.35$  MPa, the compressive modulus is  $66.35 \pm 3.88$  GPa, and the failure strain is  $1.41 \pm 0.10\%$ . All quasi-static samples indicate suspected kink band failure at the gauge section, as the composite tows after failure exhibited oblique misalignment, as marked by the red dashed line in Figure 5(a). However, due to the shielding of the resin layer, the specific failure mode needs nondestructive observation via computed tomography in the future.

The dynamic compression responses at a strain rate of  $400 \, \mathrm{s}^{-1}$  are illustrated in Figure 5(b). During the initial stage, the behavior also exhibits a linear response similar to the quasi-static one but gradually behaves a slight nonlinearity at higher loads. This may be attributed to the inherent degradation on the compression modulus of the carbon fiber monofilament [12]. The average dynamic compressive strength is  $1853.97 \pm 52.57$  MPa, the compressive modulus is  $82.53 \pm 2.78$  GPa, and the failure strain is  $2.63 \pm 0.15\%$ . Owing to the continuous loading of incident stress waves, a distinct initial compression fracture surface cannot be observed in the dynamic specimen after destroyed crush. The high-speed camera captured the initial compression failure in Figure 5(b), which was highly concentrated in a local inclined fracture. It implies the occurrence of a kink band, accompanied by the fracture of the resin layer.

The comparison of quasi-static and dynamic response, as well as the summarized properties, are illustrated in Figures 5(c) and 5(d), respectively. The longitudinal compression of the composite tow exhibits significant strain-rate dependence, as indicated by a 90% increase in compressive strength, a 24% increase in compressive modulus, and an 87% increase in failure strain from quasi-static to dynamic loading. Because the longitudinal compressive failure of UD composites is often coupled with matrix shear and microscopic interface debonding, its complex mechanism of strain-rate dependence necessitates further revelation.

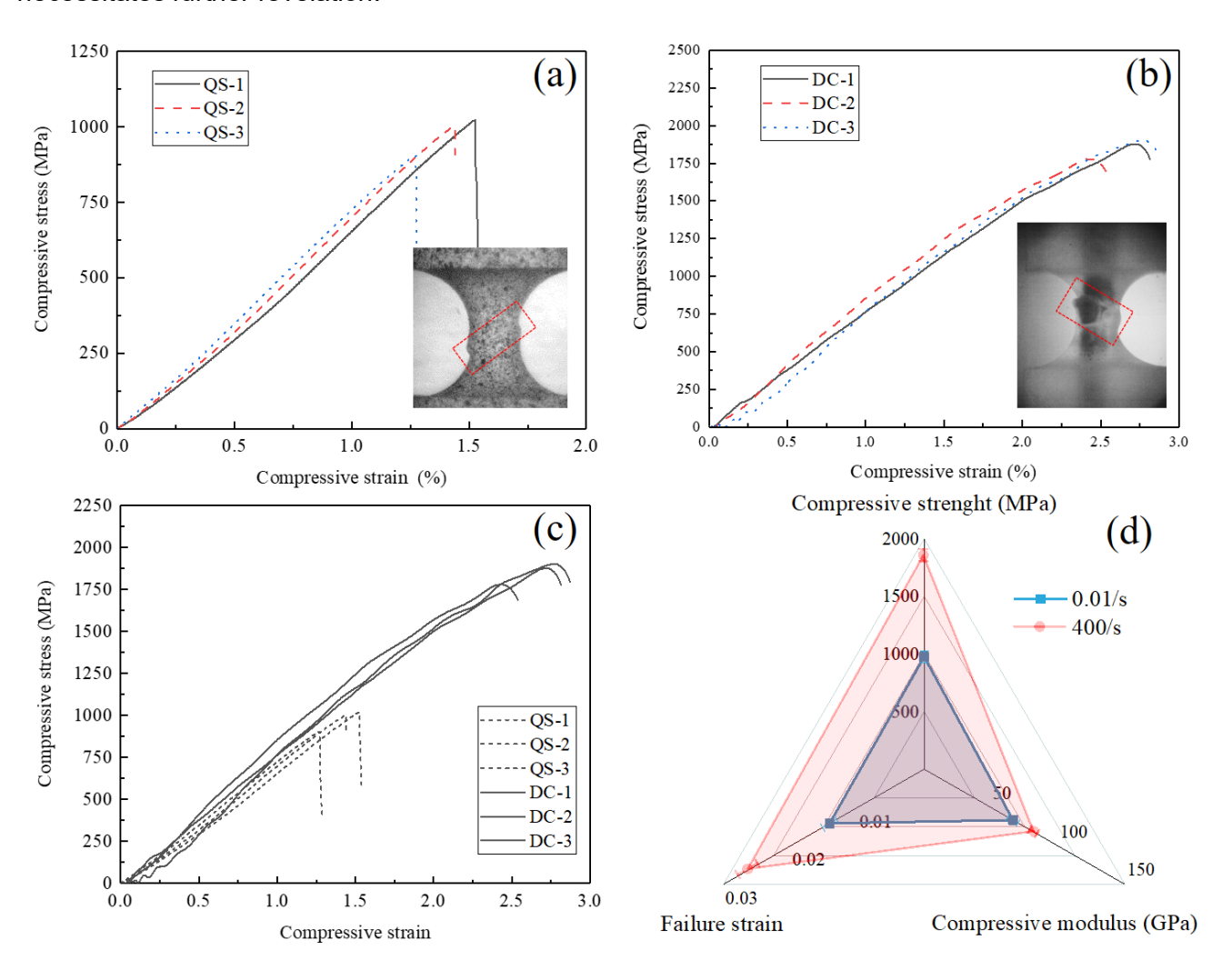


Figure 5 – Compressive results of composite tows under (a) quasi-static and (b) dynamic loadings. comparison of quasi-static and dynamic results on (c) responses and (d) properties.

### 5. Conclusions

In this study, a dynamic compression method is proposed for the mesoscopic composite tows, including material manufacturing method, specimen configuration, modified data processing methods and validation. The compressive responses of the composite tow are investigated and analyzed under 0.01/s and 400/s. Based on the current conducted research, the following main conclusions can be drawn:

- (1) Two methods for the preparation of composite tows are proposed and compared. The microscopic characterization results indicate that the pultrusion method offers more advantages than the vacuum assisted resin infusion method in terms of preparation efficiency, porosity, and surface quality.
- (2) The suitable compressive specimen configuration of composite tow was designed, and the geometric parameters of the dumbbell-shaped configuration were determined by finite element analysis. The test and simulation results of SHPB show that the specimen can achieve stress equilibrium and constant strain rate under dynamic compression.
- (3) The longitudinal compressive strength and failure strain of the composite tow exhibit a significant increase at high strain rates. Specifically, the increase in compressive strength and ultimate strain from dynamic to quasi-static loading is 90% and 87%, respectively, while the compressive modulus shows a slight increase of 24%. In all specimens, the composite tow exhibited potential kink-band failure at the peak load, occurring at the gauge section, ultimately resulting in a slanted fracture surface.

#### **Contact Author Email Address**

E-mail: <a href="mailto:zhaozhenqiang@nwpu.edu.cn">zhaozhenqiang@nwpu.edu.cn</a>
E-mail: <a href="mailto:chaozhang@nwpu.edu.cn">chaozhang@nwpu.edu.cn</a>

## **Copyright Statement**

The authors confirm that they hold copyright on all of the original material included in this paper. The authors also confirm that they have obtained permission, from the copyright holder of any third party material included in this paper, to publish it as part of their paper. The authors confirm that they give permission, or have obtained permission from the copyright holder of this paper, for the publication and distribution of this paper as part of the ICAS proceedings or as individual off-prints from the proceedings.

#### References

- [1] Shubham, C. S. Yerramalli, C. Sumant, R. K. Prusty, and B. C. Ray, "Finite element modelling and experimentation of plain weave glass/epoxy composites under high strain-rate compression loading for estimation of Johnson-Cook model parameters," *International Journal of Impact Engineering*, 2022.
- [2] H.-M. Hsiao and I. M. Daniel, "Strain rate behavior of composite materials," *Composites Part B-engineering*, vol. 29, pp. 521–533, 1998.
- [3] M. Ploeckl, P. Kuhn, J. Grosser, M. Wolfahrt, and H. Koerber, "A dynamic test methodology for analyzing the strain-rate effect on the longitudinal compressive behavior of fiber-reinforced composites," *Composite Structures*, vol. 180, pp. 429–438, 2017.
- [4] K. Rouf, M. Worswick, and J. Montesano, "Effect of strain rate on the in-plane orthotropic constitutive response and failure behaviour of a unidirectional non-crimp fabric composite," *Composites Part A: Applied Science and Manufacturing*, vol. 181, p. 108166, Jun. 2024.
- [5] Z. M. Huang, "The mechanical properties of composites reinforced with woven and braided fabrics," *Composites Science and Technology*, vol. 60, no. 4, pp. 479–498, Mar. 2000.
- [6] J. Gu, Y. Bai, Z. Zhao, and C. Zhang, "Temperature and strain rate sensitivity of modulus and yield strength of epoxy resin under compressive loads," *Polymer*, vol. 295, p. 126744, Mar. 2024.
- [7] Z. Hashin, "Failure Criteria for Unidirectional Fiber Composites," *Journal of Applied Mechanics*, vol. 47, no. 2, pp. 329–334, Jun. 1980.
- [8] J. P. Hou, N. Petrinic, C. Ruiz, and S. R. Hallett, "Prediction of impact damage in composite plates," *Composites Science and Technology*, vol. 60, no. 2, pp. 273–281, Feb. 2000.
- [9] Z. P. Bažant and B. H. Oh, "Crack band theory for fracture of concrete," *Matériaux et Construction*, vol. 16, no. 3, pp. 155–177, May 1983.
- [10] Z. Zhao, P. Liu, C. Chen, C. Zhang, and Y. Li, "Modeling the transverse tensile and compressive failure behavior of triaxially braided composites," *Composites Science and Technology*, vol. 172, pp. 96–107, Mar. 2019.
- [11] W. Wang, J. Yang, G. Q. Deng, and X. Chen, "Theoretical Analysis of Stress Equilibrium of Linear Hardening Plastic

## Dynamic compressive method for composite tows

Specimen During SHPB Tests," *Exp Mech*, vol. 63, no. 8, pp. 1353–1369, Oct. 2023. [12] M. Herráez, A. C. Bergan, C. S. Lopes, and C. González, "Computational micromechanics model for the analysis of fiber kinking in unidirectional fiber-reinforced polymers," Mechanics of Materials, vol. 142, p. 103299, Mar. 2020.